Image Stitching Method and Implementation for Immersive 3D Ink Element Animation Production

Chen Yang[1*], Siti SalmiJamali[2], Adzira Husain[3], Nianyou Zhu[4], Jian Wen[5]
School of Fashion Media, Jiangxi Institute of Fashion Technology, Nanchang, 330201, China[1]
School of Creative Industry Management and Performing Arts-College of Arts and Sciences, Universiti Utara Malaysia, 06010, Sintok, Kedah, Malaysia[1, 2, 3]
School of Architecture and Art Design, Jiangxi Technical College of Manufacturing, Nanchang, 330095, China[4]
Business School, Jiangxi Institute of Fashion Technology, Nanchang, 330201, China[5]

***Abstract*—As the growth of immersive 3D animation, its application in ink element animation is constantly updating and advancing. However, the current immersive 3D ink element animation production also has the problem of lack of innovation and repeated development, so the research innovatively designs and develops the image stitching method for immersive 3D ink element animation production. The method is designed through stereo matching algorithm and scale-invariant feature transform algorithm, and the stereo matching algorithm is optimized with the weighted median filtering method based on the guide map. In addition, the study also designs the specific implementation of this method from different functional modules. The experimental results show that on four different datasets, the error percentages of the optimized stereo matching algorithm in non-occluded areas are 0.3885%, 0.4743%, 1.6848%, and 1.34%, respectively. The error percentages of all areas are 0.8316%, 0.8253%, 4.3235%, and 4.1760%, respectively. The research and design of image stitching methods can be applied in other fields and has good practical significance.**

***Keywords*—Immersive; 3D; ink element animation; image stitching; stereo matching algorithm**

I. Introduction

As the advancement of immersive 3D animation, it has gradually become a popular form of artistic expression in animation [1]. Immersive 3D animation technology is developed on the basis of computer vision technology and image technology, and can complete its own construction through fixed steps [2]. Stereoscopic 3D animation can generate highly realistic 3D animation images by simulating the human visual system. With the development of 3D technology, the design and application of ink element animation (IEA) in 3D animation are also constantly deepening [3-4]. However, at present, the quality of immersive 3D ink element animation production enterprises is uneven, and the content produced by most enterprises is also very superficial. And this also leads to a lack of deeper thinking and spirit in the current immersive 3D ink element animation, a lack of innovation, and the problem of repeated development [5]. The current solution to the problem of missing content is to transform the existing classic 3D ink element animation into immersive 3D ink element animation, which requires the use of image stitching algorithms [6]. At present, research on image stitching algorithms mainly focuses on the stitching of monocular images, with less involvement in the stitching of binocular images. Due to the visual differences between left and right eye images, it is not appropriate to directly use monocular image stitching to process binocular images, which can affect consumers' viewing experience [7]. Based on these issues, the study innovatively designed and developed an image stitching method for immersive 3D ink element animation production, starting from the horizontal parallax dependence of stereoscopic perception. The method was designed using stereo matching algorithms and scale invariant feature conversion algorithms, and the specific implementation of the method was designed from different functional modules. The research aims to design image stitching methods for immersive 3D ink element animation production through stereo matching algorithms and scale invariant feature transformation algorithms, solve the problem of disparity, maintain the three-dimensional sense of animation, and improve the viewing experience of consumers. There are two innovative points in the research, one is the combination of stereo matching algorithm and scale invariant feature transformation algorithm, and the other is the use of weighted median filtering method to improve the stereo matching algorithm. The research is divided into four parts. The first part is a literature review, mainly involving the literature review of image stitching methods for immersive 3D ink element animation production. The second part is the specific design of image stitching methods, including image stitching algorithm design, image stitching architecture design, and functional model implementation design. The third part is the analysis of the results of the image stitching method, mainly including the performance verification of the algorithm designed by the research institute and the overall effect analysis of the image stitching method. The fourth part is the conclusion of the study, mainly summarizing and elaborating on the results of the image stitching method designed by the research institute.

II. Related Works

With the growth of immersive 3D animation technology, its own application fields are constantly expanding, and research on IS methods for immersive 3D IEA production is gradually enriching. To explore the animation of virtual medical systems, researchers such as Li designed a virtual medical system based on reality technology and 3D animation modeling. The experimental findings denoted that the calculated results under the implicit method did not increase

with the increase of the difference, and had good stability when obtaining larger values [8]. Sandoub and other experts proposed a low light level image enhancement algorithm based on fusion to avoid halo artifacts and color distortion issues when enhancing images. This algorithm estimated the illumination of low light images through the maximum color channel, and used thinning methods to improve the sharpness of the initial enhanced image. The research outcomes indicated that the proposed method was significantly superior to existing methods and reduced the issues of halo artifacts and color distortion [9]. Hosseinzadeh and other scholars proposed a new method for image centralization and pose estimation to study the creation of stitched images inside pipelines. This method would inspect and concentrate the captured video, and then generated a stitching image of the interior of the pipeline. The research findings expressed that this method had good results in IS inside pipelines [10]. Damghani and other researchers proposed an adaptive method to reduce the distortion caused by embedding information in the transformation space. This method was based on the interaction between the changes made when embedding the algorithm. The research results indicated that this method was more efficient than the most advanced methods in the field [11]. Ro and other experts put forward an in situ analysis method of mineralogy based on handheld microscope to conduct in situ analysis of mineralogy. This method solved the small observation range of microscopes through IS. The experimental outcomes denoted that this method was very effective in real-time mineralogy analysis [12].

Chen and other scholars proposed a method to convert 3D motion graphics to stereoscopic display to realize the use of stereoscopic video on mobile platforms. This method was mainly developed on the basis of animation software and output synthetic images that match the stereoscopic display. The research findings expressed that compared to traditional methods, this method had better results and faster speed in image generation [13]. Nie and other researchers proposed an IS learning framework to avoid the issue of unavailability of traditional IS methods. The framework estimated the homography through the multi-scale depth homography model, and learned the deformation rules of IS through the edge preserving deformation module. The experimental outcomes expressed that the framework had good generalization ability and was significantly superior to existing methods [14]. Dai and other experts proposed an end-to-end deep learning framework to solve the problem of artifacts when creating Panorama. This framework considered the synthesis stage in IS as a problem of image mixing and used perceptual edges to guide the network. The experimental results indicated that the framework could generate useful results in less time and had good performance [15]. Zhao and other scholars proposed an IS method based on depth homography estimation to solve the low IS accuracy. This method involved resolution and feature maps and a loss function for stitching. The experimental findings expressed that this method had good performance in quantitative evaluation and visual stitching effects [16]. Luo and other researchers proposed an IS method with constraint on the position relationship between feature points and lines to eliminate parallax. This method reduced the computation of feature matching by quickly detecting overlapping areas, and guided mesh deformation through local mesh models [17].

In summary, there is currently a wealth of research on IS methods for immersive 3D IEA production both domestically and internationally, and the methods used are also diverse. However, these studies also have certain problems, such as the lack of innovation in immersive 3D animation content, and repeated development in one direction. Therefore, the research innovatively proposes an IS method for immersive 3D IEA, constructs the method through SM algorithm and SIFT algorithm, and designs the specific implementation of the method.

III. Construction of Image Splicing Method and Design of Functional Model Implementation Method for 2D IEA Production

To construct an IS method for immersive 3D IEA, SM algorithm and SIFT algorithm are applied in the design of its functional modules. In addition, to better utilize the role of SM algorithms, a weighted median filtering method based on directional maps is used to optimize it. To design the specific implementation of the IS method functional module, the development language, library functions, and specific implementation steps of the module are studied and explained.

A. Design of IS Methods for Immersive 3D IEA Production

3D animation is a form of animation that includes computer graphics technology and is not limited by time and space conditions. 3D IEA is mainly produced through computer 3D software, which involves model building and light and shadow settings [18-19]. The production of 3D IEA should be based on its own spatial construction characteristics to achieve spatial transformation. The spatial construction characteristics of 3D IEA are shown in Fig. 1.

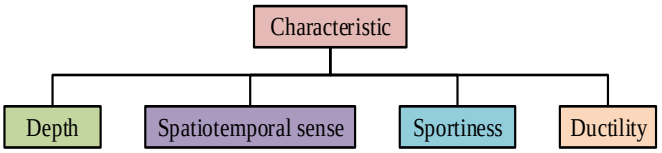

Fig. 1. The spatial construction characteristics of 3D IEA.

As shown in Fig. 1, the spatial construction characteristics of 3D IEA mainly include four points, namely stereo sense, spatiotemporal sense, motion sense, and extensibility. The stitching of immersive 3D IEA is mainly divided into seven steps. The first step is to input the image, the second step is to preprocess the data, and the third step is to register the image. The fourth step is to establish the transformation model, the fifth step is to carry out unified coordinate transformation, the sixth step is to fuse the images, and the seventh step is to obtain panoramic images. Among them, image registration and fusion are the core steps. SM algorithms can be divided into global and local SM algorithms, while the Semi Global Matching (SGM) algorithm belongs to the global algorithm [20]. The pixel level cost and smoothing constraints of the SGM algorithm are shown in Eq. (1).

$$E(D)=\sum_{p}\left(C\left(p,D_p\right)+\sum_{q\in Np}P_1T\left(\left|D_p-D_q\right|=1\right)+\sum_{q\in Np}P_2T\left(\left|D_p-D_q\right|>1\right)\right) \quad (1)$$

In Eq. (1), D denotes the disparity variable; q and p express pixels; P_1 means the penalty factor; P_2 indicates the constant penalty factor with larger values; C represents the matching cost of pixels; Np refers to adjacent pixels of pixel p; T denotes the judgment value. The calculation of P_2 is shown in Eq. (2).

$$P_2 = \frac{P_2}{\left|I_{bp} - I_{bq}\right|} \tag{2}$$

In Eq. (2), I_b indicates the reference map. When performing cost aggregation, the SGM global energy function is shown in Eq. (3).

$$E(D) = \sum_p C\left(p, D_p\right) + \sum_{q \in Np} P_1 T\left[\left|D_p - D_q\right| = 1\right] + \sum_{q \in Np} P_2 T\left[\left|D_p - D_q\right| > 1\right] \tag{3}$$

The sum of matching costs for pixels in disparity D is achieved through term $\sum C\left(p, D_p\right)$. The SGM algorithm can avoid the approximate solution of equation conversion and solve one-dimensional problems in eight directions, as shown in Eq. (4).

$$\begin{aligned} L_r(p,d) = C(p,d) + \min\left(L_r(p-r,d)\right), \\ L_r(p-r,d-1) + P_1 \\ L_r(p-r,d+1) + P_1 \\ \min\left(L_r(p-r,i) + P_2\right) - \min L_r(p-r,d+1)k \end{aligned} \tag{4}$$

In Eq. (4), r stands for a direction pointing towards the current pixel p; d expresses the value of parallax; i and k represent the pixel grayscale value.

B. IS Architecture Design for Immersive 3D IEA Production

There are three common ways to make 3D animated films, of which the first involves computer graphics technology. The second type will use parallel cameras for production, and the third type will use relevant algorithms and software [21]. To make the immersive 3D IEA better, the research uses a method that combines computer graphics technology and live shooting technology. The overall architecture of the IS system for immersive 3D IEA production is shown in Fig. 2.

As shown in Fig. 2, the IS system for immersive 3D IEA production is mainly divided into three modules, namely the 3D image source on-demand acquisition module, the ensuring parallax comfortable stitching module, and the display module. The on-demand acquisition module for stereoscopic image sources involves calculating the viewing comfort range, determining the optimal shooting position, and promoting the development of animation plots. The module for ensuring comfortable disparity stitching mainly involves depth IS, image SM, weighted median filtering, and stitching. The display module mainly includes parallax optimized line chart and panoramic effect display. When obtaining stereoscopic image sources on demand, the positioning of virtual stereoscopic cameras is mainly achieved based on the input needs of the viewer. In addition, the manipulation of scene nodes can be completed through Maya software. After the generation of stereo images, stereo perception correspondence is required, and the corresponding of stereo perception is shown in Fig. 3.

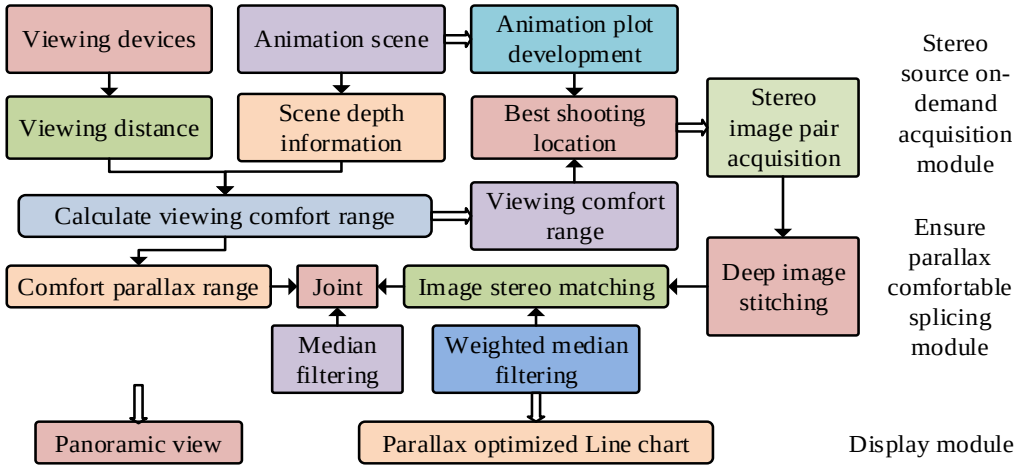

Fig. 2. The overall architecture of IS system.

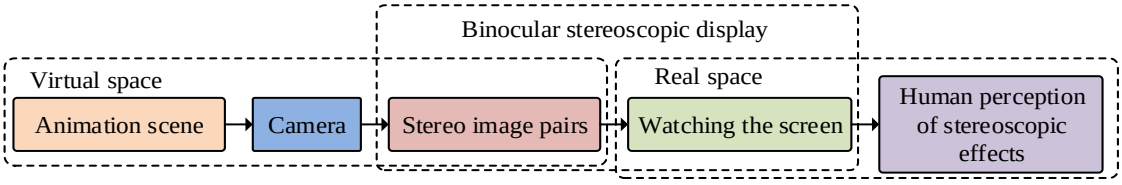

Fig. 3. The corresponding process of stereoscopic perception.

As shown in Fig. 3, the corresponding process of stereo perception is divided into three main parts: virtual space, binocular stereo display, and real space. Virtual space includes animated scenes and cameras, binocular stereo display involves stereo image pairs and viewing screens, and real space mainly includes human eye perception of stereo effects. Immersive 3D IS uses the SIFT (SIFT) algorithm, which can observe and analyze local features in images and videos. The SIFT algorithm is mainly divided into four steps. The first step is to detect the extreme values in the scale space, the second step is to locate the key points, the third step is to determine the method, and the fourth step is to describe the key points. To provide better IS functionality, the study used random sample consistency (RANSAC) algorithm and fast library for approximate nearest neighbors (FLANN) algorithm based on tree structure to optimize the SIFT algorithm. The optimization of disparity post-processing in SM algorithms is mainly achieved through the weighted median filtering (WMF) method based on directional maps [22]. This method is mainly divided into three steps. The first step is left and right consistency detection, the second step is filling in the disparity value of singular points, and the third step is smoothing the disparity value of singular points. When the matching information is insufficient, the expression of left and right consistency detection is shown in Eq. (5).

$$D_L(x,y) = D_R\left(x - D_L(x,y), y\right) \tag{5}$$

In Eq. (5), D_L denotes the left disparity map of the left eye image pair; D_R means the right disparity map of the right eye image pair; (x,y) expresses the coordinates of the interest points based on the left eye image. When the disparity value of the point in the left eye image exceeds the boundary in the right eye image, the expression of left and right consistency detection is shown in Eq. (6).

$$x - D_L(x,y) \geq 0 \tag{6}$$

To preserve the high-frequency edges of the image, the WMF method is optimized. The weight calculation involved in optimization is shown in Eq. (7).

$$W_{\partial,j}^{bf} = \frac{1}{K_\partial} e^{\left(\frac{|\partial - j|^2}{\sigma_s^2}\right)} e^{\left(\frac{|I_\partial - I_j|^2}{\sigma_c^2}\right)} \tag{7}$$

In Eq. (7), ∂ and j denote the coordinates of two points in the guidance map; σ_c and σ_s indicate constants; K_∂ is used to control the weight size; bf means the balance calculation value when the feature is f. The stereo display Comfort zone is $\left[D_{\min}, D_{\max}\right]$, and its calculation is shown in Eq. (8).

$$\begin{cases} D_{\min}(v_d) = \frac{p_d}{2}\cot(\arctan\frac{p_d}{2v_d} + \frac{|\delta\theta|}{2}) \\ D_{\max}(v_d) = \frac{p_d}{2}\cot(\arctan\frac{p_d}{2v_d} - \frac{|\delta\theta|}{2}) \end{cases} \tag{8}$$

In Eq. (8), p_d means the distance between the binocular pupils; v_d denotes the distance from the viewer to the screen; $\delta\theta$ expresses the difference between the convergence angle and the adjustment angle. The calculation of parallax at a certain point in the scene is shown in Eq. (9).

$$d = I_s \cdot f\left(\frac{1}{Z_p} - \frac{1}{D}\right) \tag{9}$$

In Eq. (9), I_s expresses the distance between the axes of the cameras; f means the focal length of the stereoscopic camera; Z_p refers to the distance from the zero parallax plane to the camera plane. The mapping relationship between the depth of the scene and the disparity at a certain point in the scene is shown in Eq. (10).

$$p(D) = I_s \cdot \left(1 - \frac{Z_P}{D}\right) \tag{10}$$

By substituting Eq. (8) into Eq. (10), the mapping relationship between parallax and viewing distance can be established, as shown in Eq. (11).

$$\begin{cases} p_{\min}(v_d) = p_d \cdot \left(1 - \frac{2v_d}{p_d \cot\left(\tan^{-1}\frac{p_d}{2v_d} + \frac{|\delta\theta|}{2}\right)}\right) \\ p_{\max}(v_d) = p_d \cdot \left(1 - \frac{2v_d}{p_d \cot\left(\tan^{-1}\frac{p_d}{2v_d} - \frac{|\delta\theta|}{2}\right)}\right) \end{cases} \tag{11}$$

If P_P is the parallax of a point in virtual space, its expression derived from the off axis model is shown in Eq. (12).

$$P_P = \left(1 - \frac{zp}{Z}\right)S \tag{12}$$

In Eq. (12), zp means zero parallax; S stands for the distance between the left and right eye cameras; Z refers to the distance between the points in the scene and the stereo camera. If the perspective of the central camera is α, the width of the projection plane is shown in Eq. (13).

$$W_p = 2 * zp * \tan\frac{\alpha}{2} \tag{13}$$

In Eq. (13), W_p is the virtual unit of length. The expression of parallax in real space is shown in equation (14).

$$P_r = \frac{W_r}{W_P} P_p \tag{14}$$

At this point, if the pixel spacing is P_p, the final disparity is shown in Eq. (15).

$$P = P_r * b \tag{15}$$

C. Design of Functional Model Implementation Methods for Immersive 3D IEA Production

To implement the functional modules of the IS method in detail, the study presents 3D IEA scenes on the basis of Maya software. During the preparation phase, the development language and library functions are set up. The Maya MEL language, which is the built-in scripting language of Maya software, is selected for development language research. The image library research selects OpenCV image library, which is powerful and has a modular structure. The functions of OpenCV can be divided into various types based on different purposes, such as video processing and graphical user interface functions. The implementation of IS method for immersive 3D IEA production is shown in Fig. 4.

In Fig. 4, the first step of the implementation of the IS method is to generate 3D image pairs, and the second step is to stitching Panorama. The third step is to generate the trget and reference Panoramas on the basis of Panorama staitching, and the fourth step is to calculate the panorama parallax. The fifth step is to optimize the seam of the current Panorama by combining the calculated panorama parallax map and the comfortable parallax range. The realization of the system function can be divided into five functional modules, namely, stereo image pair on-demand acquisition module, immersive 3D IS module, comfort zone calculation module, SM module and seam disparity optimization module. The implementation of different modules is shown in Fig. 5.

As shown in Fig. 5, the implementation of the on-demand acquisition module for stereo images mainly involves determining the position of virtual stereo cameras, which involves two methods. One is to customize the camera position by professionals, and the other is to use MEL scripting language. In addition, the rendering part is also implemented using MEL scripts. The immersive 3D IS module can achieve the acquisition of data such as the coordinates of the seam and the panoramic images of the left and right eyes through Panorama stitching of depth image pairs. In addition, the RANSAC algorithm is introduced into the findHomegraph function and used to solve the homography matrix of the image matrix. The comfort zone calculation module is mainly realized by calculating the user's viewing distance, pupil distance and other data, and the final output of the module is the range value of the comfort zone. The SM module calculates the disparity map of panoramic stereo images through the optimized SGM algorithm. The flowchart of disparity optimization at the seam is shown in Fig. 6.

In Fig. 6, the first step in optimizing the disparity at the seam is to input data into the panoramic disparity map, which mainly includes the comfortable disparity range, seam coordinate positioning, and viewing distance. The second step is to input the left Panorama into the panorama parallax map, and the panorama parallax map will return to the right Panorama based on the input data. The third step is to output the panoramic disparity map data and optimize the disparity at the seam.

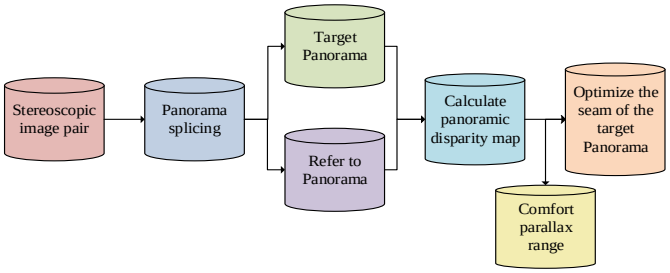

Fig. 4. Implementation of IS method.

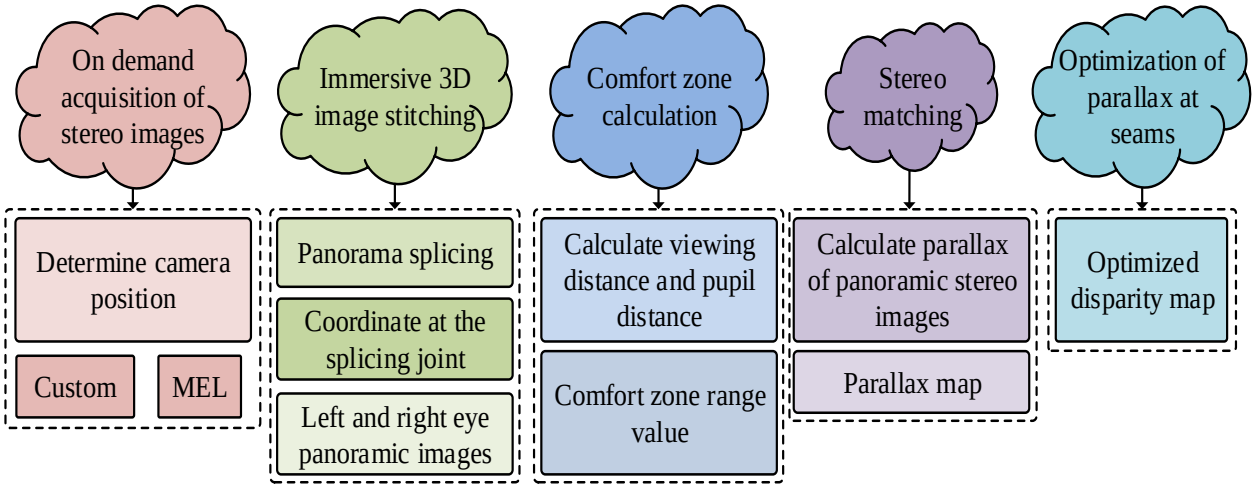

Fig. 5. Implementation of different modules.

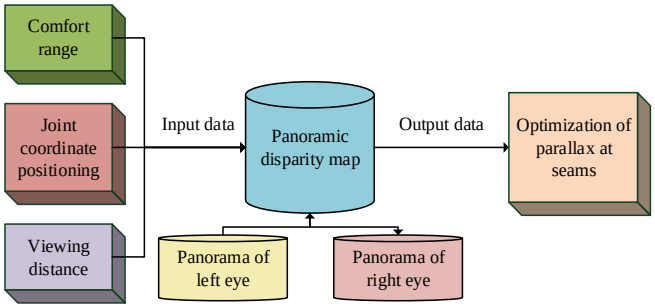

Fig. 6. Flowchart for optimizing disparity at seams.

IV. Result Analysis of IS Methods for Immersive 3D IEA Production

To analyze the results of the IS method for immersive 3D IEA production, the functional module performance and overall performance of the IS method were studied. Among them, the performance analysis of functional modules was mainly achieved by comparing F1 values and image generation error rates under different datasets. The overall performance of IS methods was mainly analyzed through runtime and rendering effects.

A. Functional Module Performance Analysis of IS Methods for 3D IEA Production

The performance testing and analysis of SM models were mainly achieved through algorithm comparison, and the selected comparison algorithms include the sum of squared differences (SSD) algorithm and the sum of absolute differences (SAD) algorithm. Four standards Middlebury stereo image datasets were selected, namely the Tsukuba, Venus, Teddy and Cones6 datasets. The comparison indicators included F1 value and error rate of image generation. The comparison of F1 values between different algorithms is shown in Fig. 7.

From Fig. 7 (a), on the Tsukuba dataset, the max, mini and average F1 value of the SGM algorithm were 0.996, 0.982 and 0.9904, respectively. The max, mini and average F1 value of the SSD algorithm were 0.885, 0.871 and 0.8794, respectively. The max, mini and average F1 value of the SAD algorithm were 0.874, 0.86 and 0.8684, respectively. From Fig. 7 (b), on the Venus dataset, the max, mini and average F1 value of the SGM algorithm were 0.996, 0.981 and 0.9902, respectively. The max, mini and average F1 value of the SSD algorithm were 0.895, 0.88 and 0.8892. The max, mini and average F1 value of the SAD algorithm were 0.891, 0.876 and 0.8852. The performance of SGM algorithm was significantly better than the other two algorithms. To analyze the performance of the optimized SGM algorithm, the study selected SGM algorithms optimized using other filtering methods for comparison, including box filtering (Box), guided filtering (Guided), and bilateral filtering (BF). The comparison of matching error percentages for different SGM algorithms under the Tsukuba and Venus datasets is shown in Fig. 8.

From Fig. 8 (a), on the Tsukuba dataset, the error percentage of the SGM, SGM+Box, SGM+Box, SGM+BF and SGM+WMF algorithms in non-occluded areas were 3.3862%, 3.2254%, 3.0173%, 2.1268% and 0.3885%, respectively. On the Venus dataset, the error percentage of non-occluded areas in the five algorithms were 0.7217%, 0.7356%, 0.2329%, 0.5478% and 0.4743%, respectively. As shown in Fig. 8 (b), the error percentage of all regions of the five algorithms on the Tsukuba dataset were 5.9688%, 4.2336%, 3.7276%, 3.2244% and 0.8316%, respectively. On the Venus dataset, the error percentages for all regions of the five algorithms were 0.9946%, 0.8234%, 0.4562%, 0.6602%, and 0.8253%, respectively. The comparison of matching error percentages for different SGM algorithms under the Teddy and Cones6 datasets is shown in Fig. 9.

From Fig. 9 (a), on the Teddy dataset, the error percentage of non-occluded areas in the SGM, SGM+Box, SGM+Guided, SGM+BF and SGM+WMF algorithms were 2.1155%, 1.9232%, 3.2346%, 1.8020% and 1.6848%, respectively. On the Cones6 dataset, the error percentages for all regions of the five algorithms were 1.9993%, 1.6732%, 2.3449%, 1.3467%, and 1.34%, respectively. From Fig. 9 (b), on the Teddy dataset, the error percentage of all regions of the five algorithms were 5.0838%, 5.1033%, 4.8143%, 4.9133% and 4.3235%, respectively. On the Cones6 dataset, the error percentages for all regions of the five algorithms were 5.9187%, 5.8999%, 5.2333%, 4.6776%, and 4.1760%, respectively.

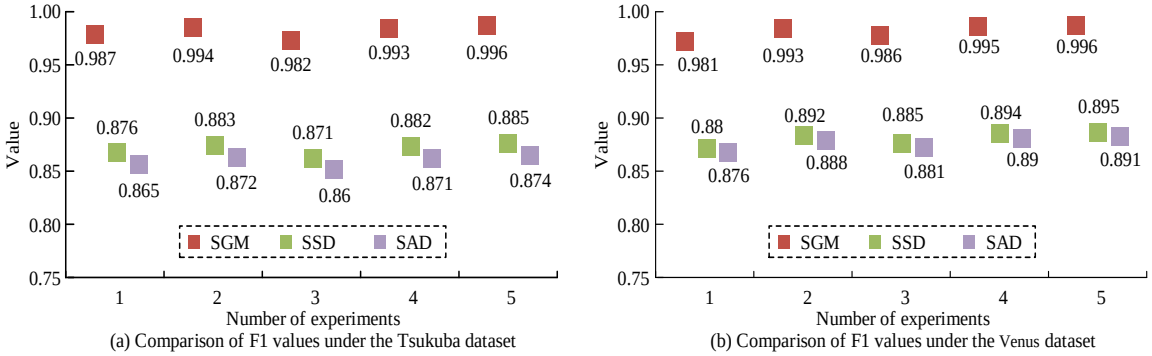

(a) Comparison of F1 values under the Tsukuba dataset

(b) Comparison of F1 values under the Venus dataset

Fig. 7. Comparison of F1 values between different algorithms.

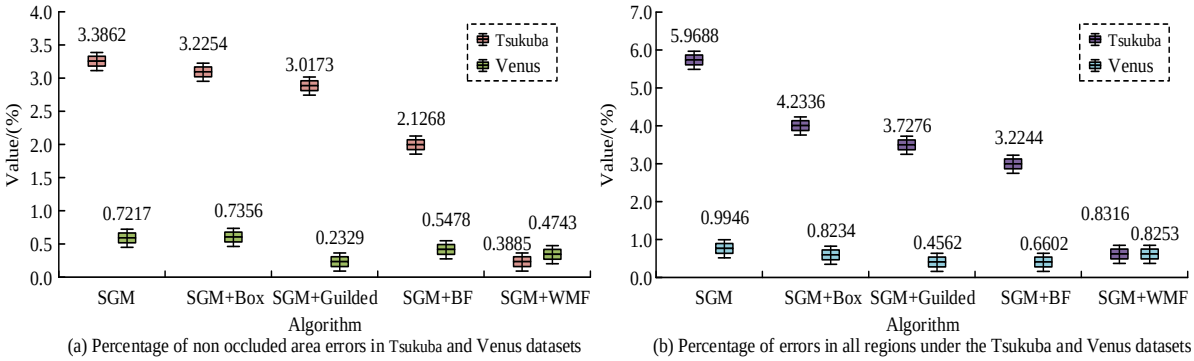

(a) Percentage of non occluded area errors in Tsukuba and Venus datasets (b) Percentage of errors in all regions under the Tsukuba and Venus datasets

Fig. 8. Comparison of matching error percentages between different SGM algorithms on the Tsukuba and Venus datasets.

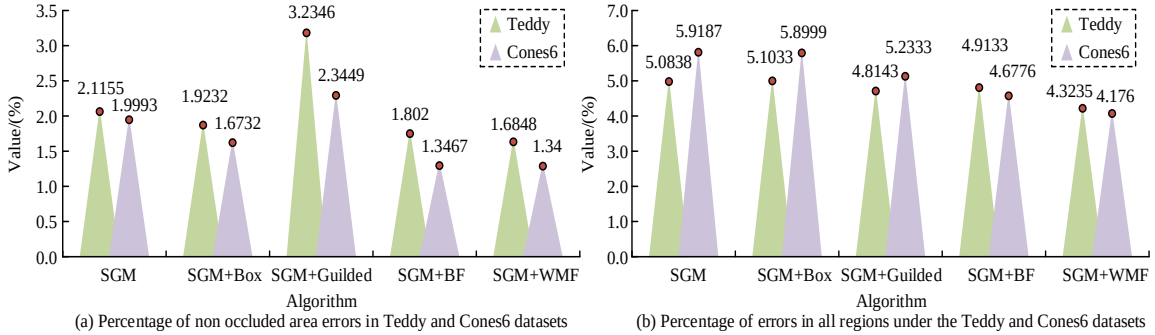

(a) Percentage of non occluded area errors in Teddy and Cones6 datasets (b) Percentage of errors in all regions under the Teddy and Cones6 datasets

Fig. 9. Comparison of matching error percentages between different SGM algorithms on the Teddy and Cones6 datasets.

B. *Overall Effect Analysis of IS Methods for 3D IEA Production*

To analyze the overall effect of IS methods for 3D IEA production; the running time of different SGM algorithms was compared. The image rendering results of the 3D IEA production IS method was mainly evaluated by observer scoring. In addition, the overall performance of the IS method was analyzed through the smoothness and restoration of the image. The comparison of the runtime of different SGM algorithms on different datasets is shown in Fig. 10.

From Fig. 10 (a), on the Tsukuba and Venus datasets, the running time of the SGM, SGM+Box, SGM+Guided and SGM+WMF algorithms were 3.7446s and 3.5657s, 4.3434s and 5.3434s, 4.5467s and 5.6884s, 5.1354s and 5.6767s, respectively. From Fig. 10 (b), on the Teddy and Cones6 datasets, the running time of the SGM, SGM+Box, SGM+Guided and SGM+WMF algorithms were 3.6586s and 3.0243s, 5.2323s and 4.9794s, 5.4245s and 5.4576s, 6.3889s and 6.7664s, respectively. In summary, although the SGM+WMF algorithm had no significant advantage in runtime, it had no impact on the overall performance of the method. The image rendering results of the 3D IEA production IS methods are shown in Fig. 11.

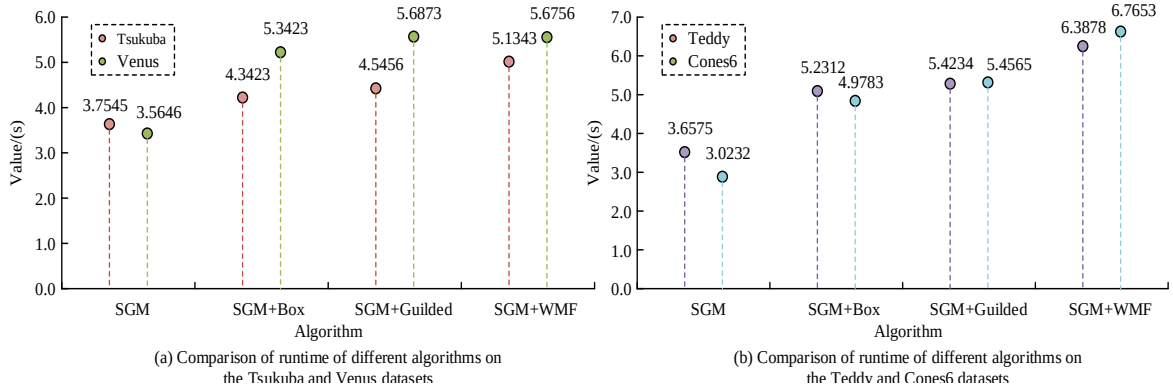

(a) Comparison of runtime of different algorithms on the Tsukuba and Venus datasets (b) Comparison of runtime of different algorithms on the Teddy and Cones6 datasets

Fig. 10. Comparison of runtime of different SGM algorithms on different datasets.

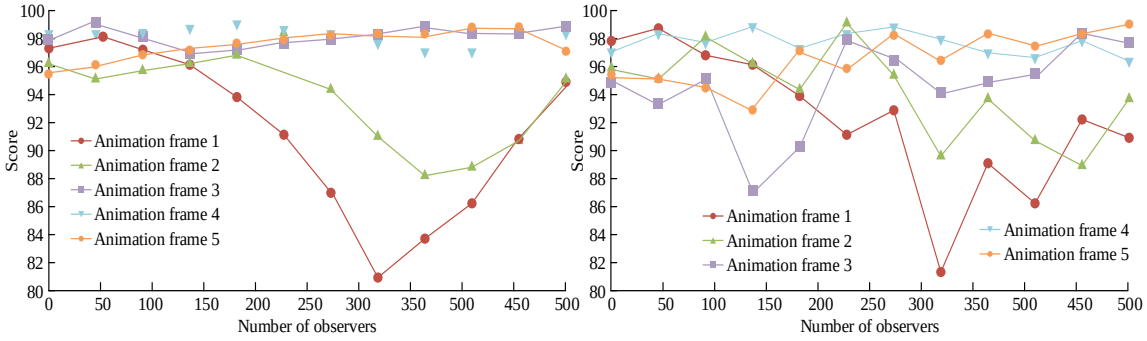

(a) The rendering score of animation 1 for 5 consecutive frames of animation (b) The rendering score of animation 2 for 5 consecutive frames of animation

Fig. 11. Image rendering results for different animations.

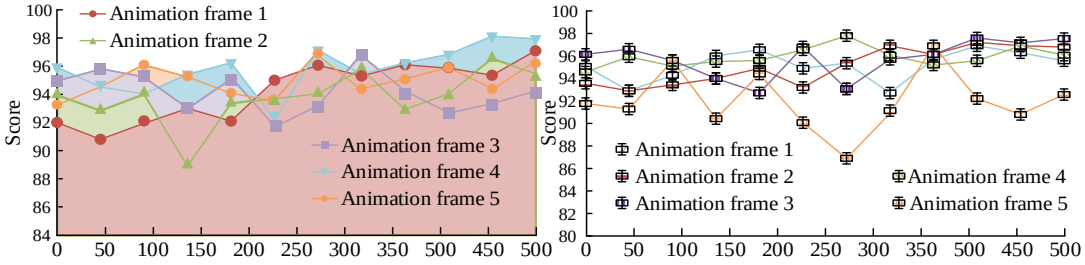

(a) Smoothness comparison of 5 consecutive frames of animation (b) Comparison of Restorability for 5 consecutive frames of animation

Fig. 12. Image smoothness and restoration.

From Fig. 11 (a), in the first ink painting animation, the max and mini rendering score of the first frame image were 98.5 and 81.3, respectively. The max and mini rendering scores for the second frame were 98.9 and 88.7, respectively. The max and mini rendering scores for the third frame were 99.5 and 97.3, respectively. The max and mini score for the fourth frame image rendering were 99.3 and 97.3, respectively. The max and mini score for the fifth frame image rendering were 99.2 and 96.5, respectively. From Fig. 11 (b), in the second IEA, the max and mini rendering score of the first frame image were 99.1 and 81.7, respectively. The max and mini rendering scores for the second frame were 99.6 and 90.1, respectively. The max and mini rendering scores for the third frame were 98.7 and 87.5, respectively. The max and mini score for the fourth frame image rendering were 99.1 and 98.1, respectively. The max and mini score for the fifth frame image rendering were 99.4 and 95.5, respectively. The image smoothness and restoration results of the 3D IEA production IS method are shown in Fig. 12.

From Fig. 12 (a), the max and mini smoothness scores of the first frame image were 96.3 and 91.2 respectively. The max and mini smoothness scores of the second frame image were 97.1 and 89.5 respectively. The max and mini smoothness scores of the third frame image were 97.2 and 92.1 respectively, while the max and mini smoothness scores of the fourth frame image were 98.4 and 94.3 respectively. The max and mini smoothness score of the fifth frame image were 97.3, and 94.5 respectively. As shown in Fig. 12 (b), the max and mini smoothness scores of the first frame image were 97.4 and 93.2 respectively. The max and mini smoothness scores of the second frame image were 97.7 and 93.5 respectively. The max and mini smoothness scores of the third frame image were 98.1 and 94.5 respectively, while the max and mini smoothness scores of the fourth frame image were 98.3 and 95.4 respectively. The max and mini smoothness score of the fifth frame image were 97.4 and 87.4 respectively.

V. Discussion

In response to the lack of content in current immersive 3D ink element animations, it is necessary to use image stitching algorithms to transform existing classic 3D ink element animations into immersive 3D ink element animations. At present, image stitching algorithms mainly focus on the stitching of monocular images, which is difficult to directly apply to the stitching of binocular images. Therefore, starting from the horizontal parallax dependence of stereoscopic perception, the research innovatively designed and developed an image stitching method for immersive 3D ink element animation production. The method was designed using stereo matching algorithms and scale invariant feature transformation algorithms, and optimized using a weighted median filtering method based on directional maps. In addition, the study also designed the specific implementation of this method from different functional modules. The analysis of the research results mainly focuses on two aspects: one is the performance verification of the algorithm used in the study, and the other is the overall effect analysis of the image stitching method. On the Tsukuba dataset, the average F1 value of the SGM algorithm is 0.9904, while the average F1 values of the SSD and SAD algorithms compared are 0.8794 and 0.8684, respectively. On the Venus dataset, the average F1 values of the three algorithms are 0.9902, 0.8892, and 0.8852, respectively. It can be seen that on different datasets, the average comprehensive evaluation value F1 of the SGM

algorithm is better than the other two comparative algorithms, indicating that the performance of the SGM algorithm is better. In the overall effect analysis of the image stitching method, the maximum rendering scores of the first ink wash animation for five consecutive frames were 98.5, 98.9, 99.5, 99.3, and 99.2, respectively. The maximum rendering scores of the second ink wash animation for five consecutive frames are 99.1, 99.6, 98.7, 99.1, and 99.4, respectively. It can be seen that the image stitching method designed by the research institute has good image rendering effects.

VI. CONCLUSION

To avoid the lack of innovation and repeated development problems existing in the current immersive 3D IEA production, an IS method was innovatively designed and developed. The method was constructed through SM algorithm and SIFT algorithm. The experimental findings showed that on four different datasets, the error percentages of the optimized SM algorithm in non-occluded areas were 0.3885%, 0.4743%, 1.6848%, and 1.34%, respectively. The error percentages of all areas were 0.8316%, 0.8253%, 4.3235%, and 4.1760%, respectively. The optimized SM algorithm had a smaller matching error rate. On four different datasets, the running time of the SGM+WMF algorithm was 5.1354s, 5.6767s, 6.3889s, and 6.7664s, respectively. The average values of image rendering scores were 90.88, 94.22, 98.6, 98.38, and 98.1, respectively. The average image smoothness values were 94.4, 93.2, 94.52, 96.62, and 95.7, respectively, while the average restoration values were 95.18, 95.36, 96.64, 96.56, and 93.36, respectively. Although research and development have been conducted on IS a method for immersive 3D IEA production, there are still certain shortcomings, such as the further improvement of SM algorithms, which can be improved in future research.

REFERENCES

[1] Lamberti F, Cannavo A, Montuschi P. Is Immersive Virtual Reality the Ultimate Interface for 3D Animators? Computer, 2020, 53(4):36-45.

[2] Somavarapu D H, Guzzetti D. Toward immersive spacecraft trajectory design: Mapping user drawings to natural periodic orbits. Acta Astronautica, 2021, 184(7): 208-221.

[3] Cen L, Ruta D, Qassem L M M S A, Ng J. Augmented Immersive Reality (AIR) for Improved Learning Performance: A Quantitative Evaluation. IEEE Transactions on Learning Technologies, 2020, 13(2): 283-296.

[4] Faisal S, Lin L. Green synthesis of reactive dye for ink-jet printing. Coloration technology, 2020, 136(2): 110-119.

[5] Huang X, Yang C, Chen Y, Zhu Z, Zhou L. Cuttlefish ink-based N and S co-doped carbon quantum dots as a fluorescent sensor for highly sensitive and selective para-nitrophenol detection. Analytical Methods, 2021, 13(44): 5351-5359.

[6] Kang Y, Wu R, Wu S, Li P, Li Q, Cao K. A novel multi-view X-ray digital imaging stitching algorithm. Journal of X-ray science and technology, 2023, 31(1):153-166.

[7] Xu J, Mou J, Liu J, Hao J. The image compression-encryption algorithm based on the compression sensing and fractional-order chaotic system. The visual computer, 2022, 38(5):1509-1526.

[8] Li L, Li T. Animation of virtual medical system under the background of virtual reality technology. Computational Intelligence, 2021, 38(1): 88-105.

[9] Sandoub G, Atta R, Ali H A, Abdel-Kader R F.A low-light image enhancement method based on bright channel prior and maximum colour channel. IET Image Processing, 2021, 15(8):1759-1772.

[10] Hosseinzadeh S, Jackson W, Zhang D, Mcdonald L, Macleod C. A Novel Centralization Method for Pipe Image Stitching. IEEE Sensors Journal, 2020, 21(10): 11889-11898.

[11] Damghani H, Mofrad F B, Damghani L. Medical JPEG image steganography method according to the distortion reduction criterion based on an imperialist competitive algorithm. IET Image Processing, 2021, 15(3): 705-714.

[12] Ro S H, Kim S H. An image stitching algorithm for the mineralogical analysis. Minerals Engineering, 2021, 169(6):106968-106979.

[13] Chen S, Jiu Z.A Method of Stereoscopic Display for Dynamic 3D Graphics on Android Platform. Journal of web engineering, 2020, 19(5): 849-863.

[14] Nie L, Lin C, Liao K, Zhao Y. Learning edge-preserved image stitching from multi-scale deep homography. Neurocomputing, 2022, 491(6): 533-543.

[15] Dai Q, Fang F, Li J, Zhang G, Zhou A. Edge-guided Composition Network for Image Stitching. Pattern Recognition, 2021, 118(9): 108019-108031

[16] Zhao Q, Ma Y, Zhu C, Yao C, Dai F. Image Stitching via Deep Homography Estimation. Neurocomputing, 2021, 450(8): 219-229.

[17] Luo X Y, Li Y, Yan J, Guan X P. Image stitching with positional relationship constraints of feature points and lines - ScienceDirect. Pattern Recognition Letters, 2020, 135(6): 431-440.

[18] Zhang G, Ling W, Duan C. Motion Damage Attitude Acquisition Based on Three-Dimensional Image Analysis. IEEE Sensors Journal, 2020, 20(20): 11901-11908.

[19] Paier W, Hilsmann A, Eisert P. Interactive facial animation with deep neural networks. IET Computer Vision, 2020, 14(6):359-369.

[20] Qi J, Liu L. The stereo matching algorithm based on an improved adaptive support window. IET image processing, 2022, 16(10): 2803-2816.

[21] Nilsson C, Nyberg J, Strmbergsson S. How are speech sound disorders perceived among children? A qualitative content analysis of focus group interviews with 10–11-year-old children. Child Language Teaching and Therapy, 2021, 37(2): 163-175.

[22] Masood F, Masood J, Zahir H, Driss K, Mehmood N, Farooq H. Novel approach to evaluate classification algorithms and feature selection filter algorithms using medical data. Journal of Computational and Cognitive Engineering, 2023, 2(1): 57-67.